Since January 2020 Elsevier has created a COVID-19 resource centre with free information in English and Mandarin on the novel coronavirus COVID-19. The COVID-19 resource centre is hosted on Elsevier Connect, the company's public news and information website.

Chemical Engineering Journal 427 (2022) 131686

Contents lists available at ScienceDirect

Chemical Engineering Journal

journal homepage: www.elsevier.com/locate/cej

Rational engineering the DNA tetrahedrons of dual wavelength ratiometric electrochemiluminescence biosensor for high efficient detection of SARS-CoV-2 RdRp gene by using entropy-driven and bipedal DNA walker amplification strategy

Zhenqiang Fan [a,1], Bo Yao [a,b,1], Yuedi Ding [a], Dong Xu [a], Jianfeng Zhao [b,*], Kai Zhang [a,*]

[a] NHC Key Laboratory of Nuclear Medicine, Jiangsu Key Laboratory of Molecular Nuclear Medicine, Jiangsu Institute of Nuclear Medicine, Wuxi, Jiangsu 214063, China
[b] Key Laboratory of Flexible Electronics (KLOFE) & Institute of Advanced Materials (IAM), Jiangsu National Synergetic Innovation Center for Advanced Materials (SICAM), Nanjing Tech University (NanjingTech), 30 South Puzhu Road, Nanjing 211816, China

ARTICLE INFO

Keywords:
SARS-CoV-2
DNA tetrahedrons
Entropy-driven
bipedal DNA walker
Ratiometric
Electrochemiluminescence biosensor

ABSTRACT

Fast and effective detection of epidemics is the key to preventing the spread of diseases. In this work, we constructed a dual-wavelength ratiometric electrochemiluminescence (ECL) biosensor based on entropy-driven and bipedal DNA walker cycle amplification strategies for detection of the RNA-dependent RNA polymerase (RdRp) gene of severe acute respiratory syndrome coronavirus 2 (SARS-CoV-2). The entropy-driven cyclic amplification reaction was started by the SARS-CoV-2 RdRp gene to generate a bandage. The bandage could combine with two other single-stranded S1 and S2 to form a bipedal DNA walker to create the following cycle reaction. After the bipedal DNA walker completed the walking process, the hairpin structures at the top of the DNA tetrahedrons (TDNAs) were removed. Subsequently, the PEI-Ru@Ti_3C_2@AuNPs-S7 probes were used to combine with the excised hairpin part of TDNAs on the surface of Au-g-C_3N_4, and the signal change was realized employing electrochemiluminescence resonance energy transfer (ECL-RET). By combining entropy-driven and DNA walker cycle amplification strategy, the ratiometric ECL biosensor exhibited a limit of detection (LOD) as low as 7.8 aM for the SARS-CoV-2 RdRp gene. As a result, detecting the SARS-CoV-2 RdRp gene in human serum still possessed high recovery so that the dual-wavelength ratiometer biosensor could be used in early clinical diagnosis.

1. Introduction

The outbreak of the new coronavirus disease 2019 (COVID-19) caused by severe acute respiratory syndrome coronavirus 2 (SARS-CoV-2) has endangered the health of people all over the world [1,2]. Before an effective vaccine is developed, in order to prevent the spread of the new coronavirus disease, the first priority is to quickly and accurately diagnose the COVID-19, especially for asymptomatic patients [3]. At present, there are two main strategies for the detection of new coronavirus diseases in the market [4]. One strategy is to detect SARS-CoV-2 RNA by using polymerase chain reaction (PCR)-based technology [5,6]. However, the operation process of PCR is complicated and different primers and temperatures need to be designed, and low accuracy usually results in false results. Another strategy is antibody-based serological and immunological testing [1]. However, after a patient being infected by SARS-CoV-2, the virus can not be detected immediately until antibodies are produced in the body. Therefore, a fast, accurate, simple, and reliable detection method is needed to detect SARS-CoV-2 to manage this epidemic. The target genomes of SARS-CoV-2 include the open reading frame 1 ab (ORF1ab) gene, nucleocapsid protein gene (N) sequence, envelope protein (E) gene, spike (S) gene, and RNA-dependent RNA polymerase (RdRp) gene [7]. These genomes play an essential role in maintaining coronavirus identity, participating in cross-reactivity with other coronaviruses, and distinguishing SARS-CoV-2 from other coronaviruses [8]. Among them, RdRp gene is a crucial catalytic component in the genomes, controlling viral RNA replication and transcription, and performs better in distinguishing SARS-CoV-2 from SARS-CoV [5]. Therefore, RdRp can be considered as an ideal target for detecting SARS-CoV-2 infection.

Compared with other detection techniques,

* Corresponding authors.
E-mail addresses: iamjfzhao@njtech.edu.cn (J. Zhao), zhangkai@jsinm.org (K. Zhang).
[1] These authors contributed equally to this work.

https://doi.org/10.1016/j.cej.2021.131686
Received 27 May 2021; Received in revised form 20 July 2021; Accepted 1 August 2021
Available online 9 August 2021

electrochemiluminescence (ECL) is widely used for the analysis of various analytes due to its high sensitivity and simplicity of operation [9,10]. The traditional ECL strategy relies on the intensity of a single signal to detect the analyte, which is easily affected by other interfering factors, such as the environment and the substrate [8,11,12]. However, ratiometric ECL using the signal ratio of the two emitters to detect the analyte can effectively avoid the interference of the environment and the substrate with improved assay accuracy [13,14]. Compared with the dual-voltage ratiometric, the dual-wavelength ratiometric ECL biosensor has two advantages: multiple co-reactants and narrow voltage ranges [15,16]. The former ECL biosensor mainly relies on the electrochemiluminescence resonance energy transfer (ECL-RET) between donors and acceptors with an improved dual signal ratio by overlapping donors' ECL emission spectrum and the acceptors' ultraviolet–visible (UV–Vis) absorption spectrum [17]. Au nanoparticles (AuNPs) have good biocompatibility and are widely used in the composite of functional nanomaterials [18]. Graphite-C_3N_4 (Au-g-C_3N_4) decorated with AuNPs has attracted attention as a donor material because of its good biocompatibility and excellent luminescence efficiency, but there is still a great lack of suitable acceptor materials [19]. Coincidentally, Ru(II) has a strong UV–vis absorption peak at 460–470 nm overlapping with the ECL emission peak of Au-g-C_3N_4. Feng et al. reported a dual-wavelength ratio ECL biosensor to detect microRNA, utilizing Au-g-C_3N_4 and $Ru(bpy)_3^{2+}$ as acceptor and donor, respectively [16]. Therefore, it is feasible to introduce Au-g-C_3N_4 as the donor and Ru(II) materials as the acceptor in the dual-wavelength ratiometric ECL biosensors.

In order to improve the sensitivity of ECL biosensors, various cyclic amplification strategies have been introduced, including hybridization chain reaction (HCR), rolling circle amplification (RCA), catalytic hairpin assembly (CHA), polymerase chain reaction (PCR) and so on [5,20–28]. These cyclic amplification strategies have complicated design processes and complicated secondary structures or require enzymes and variable temperature to participate in the reaction [29,30]. As a simple, isothermal, enzyme-free, and fast detection strategy, the entropy-driven reaction has been proposed in recent years [31,32]. An entropy-driven reaction is a kind of chain displacement reaction by acting on a toehold. Multiple hybridization and separation occur during the cycle amplification process followed by the formation of plenty of target DNAs [33–35]. In addition, the spontaneously, controllably, and continuously moveable enzyme-driven DNA walker on the track was introduced into biosensors as an amplification strategy [36]. Yuan's research group used a single-step DNA walker to detect miRNA-141 [37]. Lei and his colleagues designed a single-step, two-site DNA walker to detect the target DNA [38]. However, walking efficiency cannot be improved due to the limited walking space of the single-step DNA walker. By contrast, the bipedal DNA walker has ample walking space and high efficiency [39]. Therefore, the simultaneous introduction of entropy-driven and bipedal DNA walker amplification strategies can significantly improve the sensitivity of the biosensor.

The electrode surface constructed by DNA tetrahedrons (TDNAs) can reduce the background signal and improve the hybridization efficiency of the target DNA [2]. One of the four single strands of each TDNA, the longest single strand can be designed to bind to the target DNA [40], possessing the advantages of easy synthesis, muscular mechanical rigidity, and uniform distribution of captured probes electrode surface [40]. Li et al. designed a multi-functional TDNA-based microarray platform that can be used to detect let-7a miRNA, prostate-specific antigen, and cocaine [41]. Lin et al. constructed a TDNAs sensor to detect Golgi protein 73 (GP73) [42]. The DNA tetrahedral sensor has a higher ECL signal compared to the single-stranded probe that detects GP73. The background signal of the TDNAs sensor is lower when there is no target present in the system, which is because the biosensor constructed from TDNAs can effectively prevent non-specific adsorption and significantly improve the detection sensitivity of the system.

In this work, we constructed a TDNAs-based dual-wavelength ratiometric biosensor combined with entropy-driven and bipedal DNA walker amplification strategies to detect the SARS-CoV-2 RdRp gene. First of all, the Au-g-C_3N_4 modified on the electrode surface possessed strong ECL emission at 460 nm. And a large number of TDNAs with a hairpin structure as the bipedal DNA walker's trackies were modified on the surface of Au-g-C_3N_4. Secondly, by using the SARS-CoV-2 RdRp gene as a catalyst to trigger an entropy-driven reaction, the bandage was output, which could combine with two single-stranded S1 and S2 to form a bipedal DNA walker. It is worth mentioning that when the bandage is not introduced, even if 3′ terminus of the single-stranded S1 or S2 and the hairpin DNA are base-paired, their melting temperature (T_m) is too low to bind with each other. However, single-stranded S1 and S2 are induced by the bandage to form a bipedal DNA walker (S1 and S2 are used as the two feet of the bipedal DNA walker), resulting in a closer distance between single-stranded S1 and S2. This combination increased the T_m of the two feet of the bipedal DNA walker and the hairpin DNA [43]. Next, the bipedal DNA walker spontaneously moved on the hairpin structure at the top of the TDNAs with the help of Nb.BbvCI endonuclease, causing a large number of hairpin structures to be removed. Finally, a PEI-Ru@Ti_3C_2@AuNPs-S7 probe was synthesized to combine with the top of the TDNAs giving a strong ECL emission at 620 nm through the ECL-RET. The sensitivity of this ECL biosensor can be improved by the above-mentioned multi-step reaction. Experiments in human serum also demonstrated a high recovery rate, indicating that this biosensor could provide a reference value for early clinical diagnosis.

2. Experimental section

2.1. Chemicals and materials

Gold chloride trihydrate ($HAuCl_4{\cdot}3H_2O$), sodium citrate, potassium persulfate ($K_2S_2O_8$) and sodium borohydride ($NaBH_4$) were obtained from Aladdin Biochemical Technology Co. Ltd. (Shanghai, China). Ti_3C_2 dispersion liquid and g-C_3N_4 were obtained from Jiangsu XFNANO Materials Tech, Co. Ltd. (Nanjing, China). Tris (4,4′-dicarboxylic acid-2,2′-bipyridyl)ruthenium (II) dichloride ($Ru(dcbpy)_3Cl_2$) was obtained from Suna Tech Inc. (Suzhou, China). Tris(2-carboxyethyl)phosphine hydrochloride (TCEP) and 6-mercaptohexanol (MCH) were gained from Sigma-Aldrich (St Louis, MO, USA). Nb.BbvCI and 10 × NEB buffer were obtained from New England Biolabs (USA). The purified DNA sequences (Table S1) were synthesized by Genscript Bio-technology Co. Ltd. (Nanjing, China). Real human sera were collected from healthy volunteers at the Jiangyuan Hospital affiliated with Jiangsu Institute of Nuclear Medicine. And the medical ethical approval procedure was followed in the recovery experiment of SARS-CoV-2 RdRp assay, and consent was obtained from the subjects.

2.2. Instrumentation

Transmission electron microscopy (TEM) images were obtained from a JEM-2100F, JEOL (Japan). Cyclic voltammetry (CV) and electrochemical impedance spectroscopic (EIS) were measured by an electrochemical workstation (Shanghai Chenhua Instruments Co., China), performing in 5.0 mM $[Fe(CN)_6]^{3-/4-}$ solution. ECL signals were captured by ECL-6B belonging to the State Key Laboratory of Analytical Chemistry for Life Sciences, Nanjing University. UV–Vis absorption spectrum was measured by Microplate Reader (Spectra Max M5e) with a range of 250 nm to 700 nm (Molecular Devices Co. Ltd, USA). Atomic force microscope (AFM) images were obtained from Dimension ICON (Bruker). The gel image was photographed by Bio-Rad ChemDoc XRS.

2.3. Preparation of the Au-g-C_3N_4

We successfully synthesized Au-g-C_3N_4 with reference to other people's literature and made some changes [16]. In simple terms, 50 μL of

$HAuCl_4$ (0.01 M) solution and 4 mL of g-C_3N_4 (0.15 mg mL^{-1}) were mixed and sonicated for 10 min, followed by stirring for 1 h. Then, 100 μL of fresh $NaBH_4$ (0.01 M) solution was injected into the mixed solution and treated in an ice bath for 20 min. Continuously, 50 μL of sodium citrate solution was added to the above-mixed solution, and the hybrid solution was continuously stirred at 25 °C for 20 min. Finally, to remove the excess AuNPs, sodium citrate and $NaBH_4$, the above-mixed solution was washed and sonicated three times to obtain pure Au-g-C_3N_4, which was redispersed in 1 mL of H_2O and stored at 4 °C for the next experiment.

2.4. Preparation of the PEI-Ru@Ti_3C_2@AuNPs-S7

The PEI-Ru@Ti_3C_2@AuNPs-S7 probe was successfully synthesized with slight modification by referring to others' literature [44]. 10 mg of $Ru(dcbpy)_3^{2+}$ and EDC (200 mM)/NHS (50 mM) were simultaneously dissolved in 5 mL of PBS (0.1 M, pH = 7.4) with continuous stirring for 2 h. The Ti_3C_2 suspension and PEI (1%, w/v) were mixed well and added to the PBS (0.1 M, pH = 7.4) of $Ru(dcbpy)_3^{2+}$ for 1 h. Subsequently, 600 μL of $HAuCl_4$ (0.01 M) and 600 μL of fresh $NaBH_4$ (0.01 M) were added to the above solution and stirred for 1 h. The prepared PEI-Ru@Ti_3C_2@AuNPs were then centrifuged, washed three times to remove excess impurities and finally redispersed in 1 mL of PBS (0.1 M, pH = 7.4). For further preparing PEI-Ru@Ti_3C_2@AuNPs-S7 probes, 200 μL of S7 (10 μM) to 1 mL of Ru@Ti_3C_2@AuNPs was added and stored in a refrigerator at 4 °C for overnight. Finally, 100 μL of MCH (100 μM) was added to reduce non-specific adsorption. In this way, the preparation of the PEI-Ru@Ti_3C_2@AuNPs-S7 probe was made.

2.5. Preparation of TDNAs

The construction of TDNAs was based on previous literature with slight modifications[45]. Briefly, 10 μL of the four single-stranded DNAs (S3, S4, S5, S6) were dissolved in PBS buffer (pH = 7.4) containing 10 mM TCEP and 50 mM $MgCl_2$. Then, the four single-stranded DNAs were mixed and placed at 95 °C for 5 min, cooled to room temperature, and stored for 3 h in turn. Finally, sturdy TDNAs were obtained.

2.6. Polyacrylamide gel electrophoresis (PAGE) analysis

First of all, the prepared 20 % polyacrylamide gel run at 80 V for 40 min. Next, 10 μL of DNA sample (1 μM) and the loading buffer were mixed and injected into the gel sample tank and run at 110 V for 2.5 h. Then, 20 % of the gel was soaked in the Gel-Red diluent for 30 min. Finally, the stained gel was photographed by ChemiDoc MP Imager instrument. The gel electrophoresis experiments could prove the construction process of TDNAs, the entropy-driven reaction process, and the bipedal DNA walker.

2.7. Procedure of entropy-driven cycle amplification reaction

The SARS-CoV-2 RdRp gene initiated the reaction to generate a lot of bandage through the entropy-driven cyclic amplification reaction. Initially, 150 μL of three DNA strands, blocker (0.4 M), bandage (0.4 M), and scaffold (0.4 M) were placed at 95 °C for 5 min and slowly cooled to room temperature, so that a ternary structure of substrate could be formed. Then, various concentrations of the SARS-CoV-2 RdRp gene were added to the system and incubated at 25 °C. In this way, the early-formed intermediate 1 transformed to intermediate 2 while the bandage was released during the process. Simultaneously, 50 μL of the fuel chain (0.4 M) was added to the mixed solution and incubated at 25 °C for 40 min. As a result, a binary waste chain was formed and the SARS-CoV-2 RdRp gene was released to continually participate in the next cycle reaction.

2.8. Fabrication of the ratiometric ECL biosensor

At first, the glassy carbon electrode (GCE) was cleaned according to the previous method [46]. 10 μL of Au-g-C_3N_4 was imprisoned on GCE to obtain Au-g-C_3N_4/GCE, and dried at room temperature. Subsequently, the resulting Au-g-C_3N_4/GCE was immersed in 100 μL of TDNAs (1 μM) solution containing 10 mM TCEP for 8 h to reduce the S-S bond. Next, the modified GCE was immersed in 60 μL of MCH (100 μM) solution for one h to prevent non-specific adsorption. Then, the modified MCH/$TDNA_S$/Au-g-C_3N_4/GCE was incubated at 37 ℃ in the entropy-driven reaction mixture for 60 min (including different concentrations of SARS-CoV-2 RdRp gene). And the two single-stranded S1 (60 nM), S2 (60 nM) and Nb.BbvCI (10 U) was added into the mixed solution simultaneously, followed by the completed walking process of the DNA walker on the electrode surface. Finally, the synthesized PEI-Ru@Ti_3C_2@AuNPs-S7 probe was dropped on the surface of the modified electrode giving PEI-Ru@Ti_3C_2@AuNPs-S7/MCH/TDNAs/Au-g-C_3N_4/GCE, which was dried at room temperature. In each step mentioned above, PBS solution was required to wash off the unconnected substances. The constructed electrode was stored in a refrigerator at 4 °C for the next experiment.

2.9. Analysis procedure

The prepared electrode was placed in 5 mL of PBS (pH = 7.4) containing $S_2O_8^{2-}$ (0.1 M) for the experiment, the ECL signal was captured by ECL-6B, and the scanning range was from −1.5–0 V. EIS and CV were measured by using the electrochemical workstation. A three-electrode system was used for testing, with modified 3 mm GCE as the working electrode, platinum wire electrode as the counter electrode and Ag/AgCl as the reference electrode.

3. Results and discussion

3.1. Mechanism of ratiometric ECL biosensor

We synthesized a ratiometric ECL biosensor to detect the SARS-CoV-2 RdRp gene based on entropy-driven and DNA walker's cyclic amplification strategies. The principle of entropy-driven and DNA walker amplification strategy was shown in Scheme 1. SARS-CoV-2 RdRp gene acts as a trigger to start cycle 1. With the help of the toehold of the substrate (consisting of the three chains of the scaffold, blocker, and bandage), SARS-CoV-2 RdRp can be combined with the scaffold to form an intermediate 1. At this time, since the binding force of the bandage and scaffold is weak, the bandage is released and the intermediate 1 transformed into intermediate 2. The exposed toehold of intermediate 2 is combined with fuel to produce double-stranded waste, blocker, and SARS-CoV-2 RdRp gene acting as a catalyst to stimulate the next cycle.

After many cycles, a large amount of bandage is exported. Subsequently, Strand 1, Strand 2, and bandage combine to form a bipedal DNA walker in order to initiate cycle 2. Initially, the TDNAs were modified on the surface of Au-g-C_3N_4/GCE to obtain a strong ECL signal at 460 nm. In the presence of Nb.BbvCI endonuclease, the bipedal DNA walker can spontaneously walk on the hairpin at the top of the TDNAs. As a result, a large number of hairpins on top of the TDNAs are removed and bind specifically to the PEI-Ru@Ti_3C_2@AuNPs-S7 probe. Through ECL-RET, the ECL signal at 460 nm was quenched and at 620 nm was generated. The SARS CoV-2 RdRp gene can be quantitatively detected based on the degree of decrease in ECL signal at 460 nm and the increase in ECL signal at 620 nm. Combining with two signal amplification strategies, the ratiometric ECL biosensor has efficiently detected the SARS-CoV-2 RdRp gene.

3.2. Construction of the Dual-Wavelength ratiometric ECL-RET biosensor

The ratiometric ECL biosensor was designed based on the ECL-RET

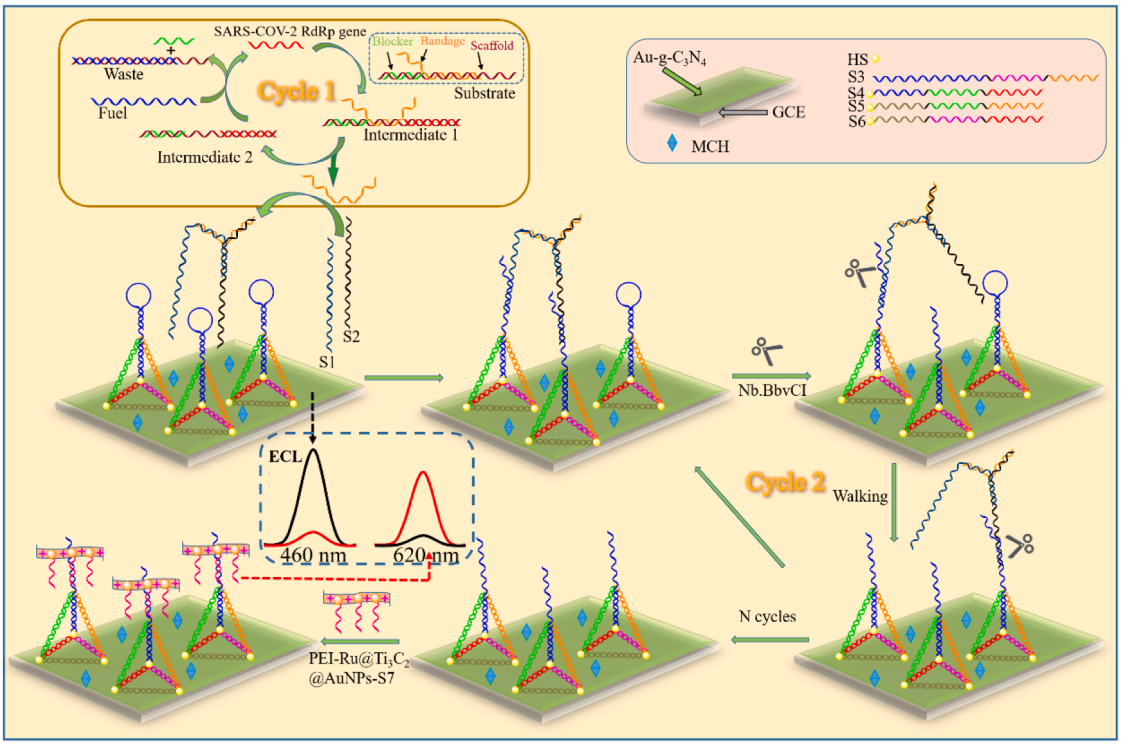

Scheme 1. Schematic illustration of the entropy-driven and bipedal DNA walker amplification strategies based DNA tetrahedral ratiometric ECL biosensor for the assay SARS-CoV-2 RdRp gene.

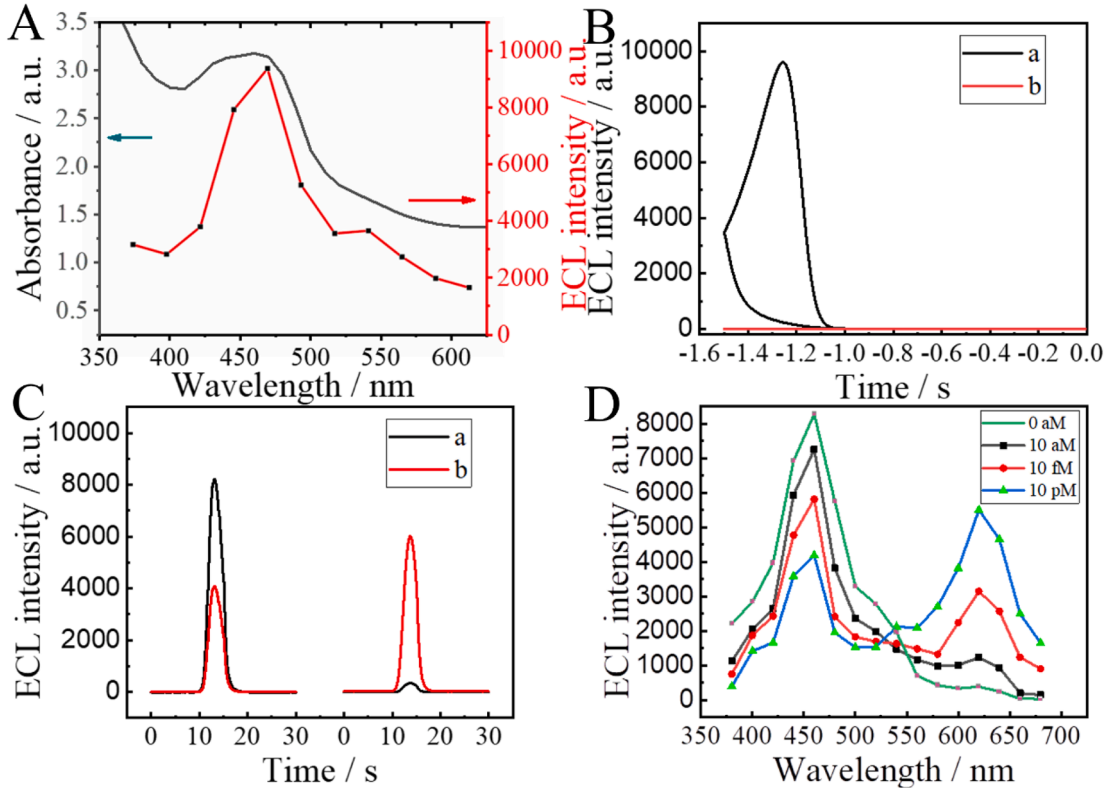

Fig. 1. (A) UV–Vis absorption spectrum of PEI-Ru@Ti_3C_2@AuNPs (gray curve) and ECL spectrum of Au-g-C_3N_4 (red curve), ECL curves were obtained through a series of filters, measured in 0.1 M PBS (pH = 7.4) containing 0.1 M $S_2O_8^{2-}$. (B) ECL spectrum of GCE/Au-g-C_3N_4 (curve a) and GCE/PEI-Ru@Ti_3C_2@AuNPs (curve b), scanned at −1.5–0 V. (C) ECL signal intensity of (a) GCE/Au-g-C_3N_4/TDNAs/MCH, (b) GCE/Au-g-C_3N_4/TDNAs/MCH treated with 10 pM of SARS CoV-2 RdRp and further incubated with PEI-Ru@Ti_3C_2@AuNPs-S7. (D) Ratiometric ECL biosensor at different concentrations (0 aM, 10 aM, 10 fM, and 10 pM) of SARS CoV-2 RdRp was tested using a series of filters spaced 20 nm apart, measured in 0.1 M PBS (pH = 7.4) containing 0.1 M $S_2O_8^{2-}$. (For interpretation of the references to colour in this figure legend, the reader is referred to the web version of this article.)

principle between Au-g-C_3N_4 and PEI-Ru@Ti_3C_2@AuNPs. As was shown in Fig. 1A, the ECL emission spectrum of Au-g-C_3N_4 matched well with the UV–Vis absorption spectrum of PEI-Ru@Ti_3C_2@AuNPs. It was indicated that ECL-RET could be achieved between Au-g-C_3N_4 donor and PEI-Ru@Ti_3C_2@AuNPs acceptor. In addition, when the sensing system was scanned with a voltage from −1.5–0 V in the presence of $S_2O_8^{2-}$, there was an ECL emission peak on the Au-g-C_3N_4/GCE (Fig. 1B). However, the absence of ECL emission peak from PEI-Ru@Ti_3C_2@AuNPs/GCE indicated that the PEI-Ru@Ti_3C_2@AuNPs acceptor has not interfered with the ECL emission of Au-g-C_3N_4 donor at the cathode voltage. Fig. 1C showed the ECL intensity change curve before and after modification of the PEI-Ru@Ti_3C_2@AuNPs-S7 probe. A powerful ECL signal at 460 nm and a weak ECL signal at 620 nm appeared when the electrode was not modified with the PEI-Ru@Ti_3C_2@AuNPs-S7 probe. On the contrary, a weak ECL signal appeared at 460 nm and a powerful ECL signal appeared at 620 nm when the electrode was modified with the PEI-Ru@Ti_3C_2@AuNPs-S7 probe. It was further indicated that the ECL-RET between the Au-g-C_3N_4 donor and PEI-Ru@Ti_3C_2@AuNPs acceptor was reasonable. As displayed in Fig. 1D, a series of filters was used to explore the changes in ECL intensity with the increase of SARS-CoV-2 RdRp concentrations. When the SARS-CoV-2 RdRp was absent in the system, only the ECL emission peak appeared at 460 nm. However, as the concentration increased, the intensity of the ECL signal at 460 nm gradually decreased, and accordingly the ECL emission peak continued to increase at 620 nm. These results successfully demonstrated that the ratiometric biosensor of the ECL-RET could effectively detect the SARS-CoV-2 RdRp gene.

3.3. Possible luminescence mechanism about ECL biosensor

Referring to the previous luminescence mechanism of g-C_3N_4, the modified electrode was placed in the PBS solution containing 0.1 M $S_2O_8^{2-}$, and the scanning voltage was from −1.5–0 V. The possible luminescence mechanism is as follows equation (1) - (4). Firstly, g-C_3N_4 acquires an electron to become g-$C_3N_4^{\bullet-}$ (equation 1). Secondly, $S_2O_8^{2-}$ is reduced to SO_4^{2-} and $SO_4^{\bullet-}$ (equation 2). Then electron transfer occurs between $SO_4^{\bullet-}$ and g-$C_3N_4^{\bullet-}$, and then the g-$C_3N_4^{\bullet-}$ becomes excited state g-C_3N_4* (equation 3). Eventually, the excited state g-C_3N_4* becomes the ground state g-C_3N_4 to generate light (460 nm) (equation 4).

$$g - C_3N_4 + e^- \rightarrow g - C_3N_4^{\bullet-} \quad (1)$$

$$S_2O_8^{2-} + e^- \rightarrow SO_4^{\bullet-} + SO_4^{2-} \quad (2)$$

$$g - C_3N_4^{\bullet-} + SO_4^{\bullet-} \rightarrow g - C_3N_4^{*} + SO_4^{2-} \quad (3)$$

$$g - C_3N_4^{*} \rightarrow g - C_3N_4 + h\nu \quad (460\ \text{nm}) \quad (4)$$

3.4. Characterization of Au-g-C_3N_4

It can be seen from Fig. 2A AuNPs with a diameter size of 8 ± 1 nm were uniformly dispersed on the surface of Au-g-C_3N_4. Fig. 2B was an energy dispersive X-ray (EDX) analysis. The results showed that the element peaks of C, N, and Au existed in the EDX spectrum of Au-g-C_3N_4, while the element peak of Au was not observed in the EDX spectrum of g-C_3N_4 (shown in the inset of Fig. 2B). The UV–Vis absorption spectrum was used to characterize Au-g-C_3N_4, as shown in Fig. 2C. Among them, g-C_3N_4 and AuNPs show characteristic peaks at around 360 nm and 520 nm, respectively. The prepared Au-g-C_3N_4 contained two characteristic peaks, which proved that Au-g-C_3N_4 was successfully synthesised. The ECL property of Au-g-C_3N_4 was verified in Fig. 2D. The ECL signal intensity of Au-g-C_3N_4 (curve b) was greater than that of g-C_3N_4 (curve a),

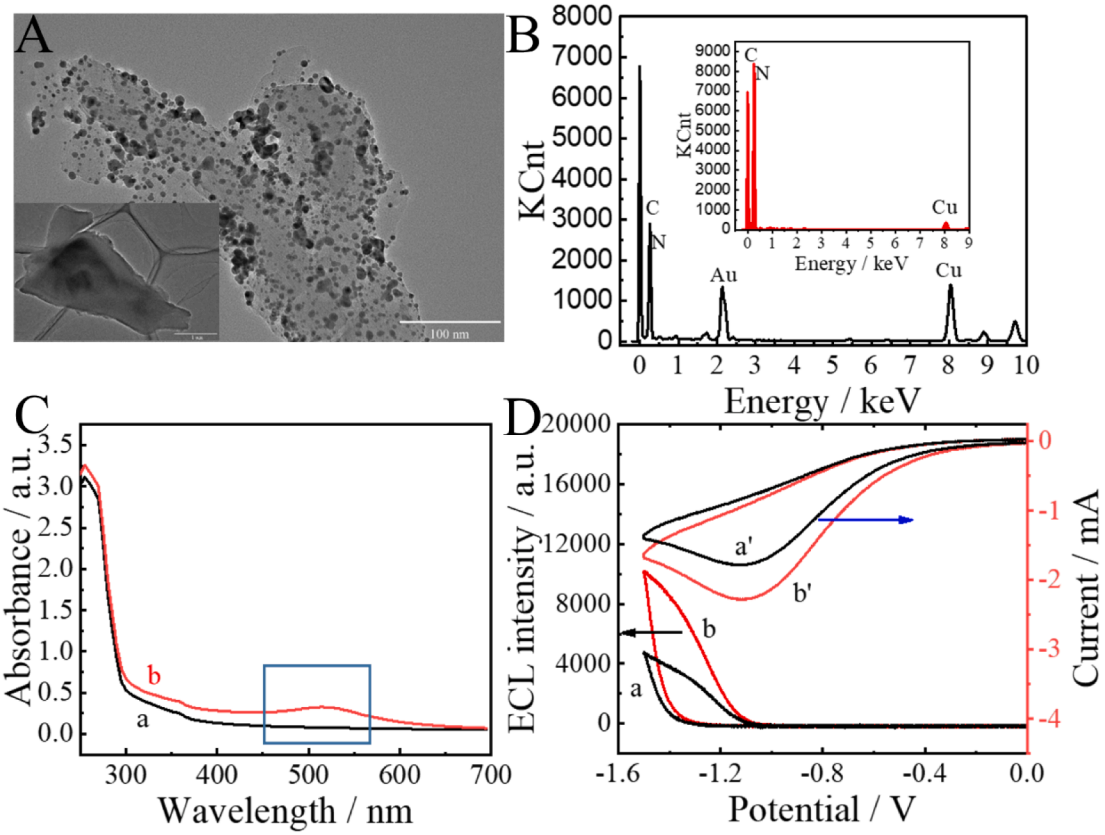

Fig. 2. (A) TEM characterization of Au-g-C_3N_4, inset shows g-C_3N_4. (B) EDX spectrum of Au-g-C_3N_4, inset shows EDX of g-C_3N_4. (C) UV–vis absorption spectrum of g-C_3N_4 (curve a) and Au-g-C_3N_4 (curve b). (D) ECL intensity curves of g-C_3N_4 (curve a) and Au-g-C_3N_4 (curve b), cyclic voltammetry curves of g-C_3N_4 (curve a') and Au-g-C_3N_4 (curve b'), modified on GCE tested in 0.1 M PBS (pH = 7.4) containing 0.1 M $S_2O_8^{2-}$.

which benefited from the outstanding conductivity of AuNPs. The CV curve also verified that Au-g-C_3N_4 (curve b') possessed brilliant conductivity compared with single-component g-C_3N_4 (curve a').

3.5. Characterization of PEI-Ru@Ti_3C_2@AuNPs

Fig. 3A showed the TEM characterization of monolayer Ti_3C_2. From Fig. 3B, it can be seen that the AuNPs were uniformly dispersed on the surface of Ti_3C_2, and there was no aggregation, which indicated that Ti_3C_2 as an excellent carrier could prevent the accumulation of AuNPs. As seen in Fig. 3C, the diameter of AuNPs was 4.5 ± 1 nm. The PEI-Ru@Ti_3C_2@AuNPs nanocomposites characterized by EDX (see Fig. 3D) showed elemental peaks of C, N, O, Ti, Au, Ru, indicating that the PEI-Ru@Ti_3C_2@AuNPs nanocomposites were successfully synthesized. Besides, we verified the synthesis of PEI-Ru@Ti_3C_2@AuNPs with UV–vis characterization, as shown in Fig. S1. The characteristic absorption peaks of Au nanoparticles are around 525 nm, and the characteristic absorption peaks of $Ru(dcbpy)_3^{2+}$ are around 300 nm and 475 nm. PEI-Ru@Ti_3C_2@AuNPs has both Au and $Ru(dcbpy)_3^{2+}$ absorption peaks, which further verifies the successful synthesis of ECL acceptor materials.

3.6. Characterization of TDNAs

Polyacrylamide gel electrophoresis (PAGE) was used to demonstrate the process of TDNAs construction, as shown in Fig. 4A. Lane 1 to Lane 4 was the construction process from single-stranded S1 to four-stranded TDNAs. It can be seen from gel that as the number of DNA strands gradually increased, the corresponding band was further behind, which was consistent with the expected result. AFM was used to characterize TDNAs. In Fig. S2, the height of the TDNAs were 5 ± 0.2 nm, which is almost consistent with the theoretical value of 5.27 nm. This is further evidence that the TDNAs were successfully constructed.

3.7. Characterization of entropy-driven and bipedal DNA walker

PAGE was used to verify the entropy-driven reaction shown in Fig. 4B. The bands of scaffold, blocker and bandage were shown in Lane 1, Lane 2 and Lane 3, respectively. Lane 4 showed the band of the substrate formed by scaffold, blocker and bandage. By introducing SARS-CoV-2 RdRp, the substrate was converted into intermediate 2 and bandage with the help of toehold, and two new bands could be seen generated in Lane 5. Next, by introducing substrate, SARS-CoV-2 RdRp and fuel in the system, eventually generating binary waste, bandage and blocker could be observed in Lane 6, but the band of SARS-CoV-2 RdRp was not seen as involved in the next cycle.

Fig. 4C reflected the construction of the bipedal DNA walker. When there was no bandage in the system, S1 and S2 cannot combine with each other (Lane 3), and the position of the band was consistent with a single S1 (Lane 1) or S2 (Lane 2). However, when there was bandage in the system and S1 and S2 could form a bipedal DNA walker, the molecular weight was larger, and the band position was later in the gel. Therefore, it proved that by introducing bandage, bipedal DNA walker was successfully constructed.

3.8. Effects of material modifications on the performance of the electrodes

The CV was used to characterize the construction process of the biosensor in Fig. 5A. The bare electrode (curve a) maintained the most prominent current peak. When Au-g-C_3N_4 (curve b) was deposited on the electrode surface, the current peak decreased. Then continued to modify the TDNAs (curve c) and MCH (curve d) on the electrode, the current peak continued to decline that the surface of the electrode adsorbed substances with poor conductivity. When SARS-CoV-2 RdRp and Nb.BbvCI were introduced (curve e), the walking process of DNA walker was completed on the electrode surface. As a result, TDNAs were excised and the peak current increased. Finally, the specific binding of

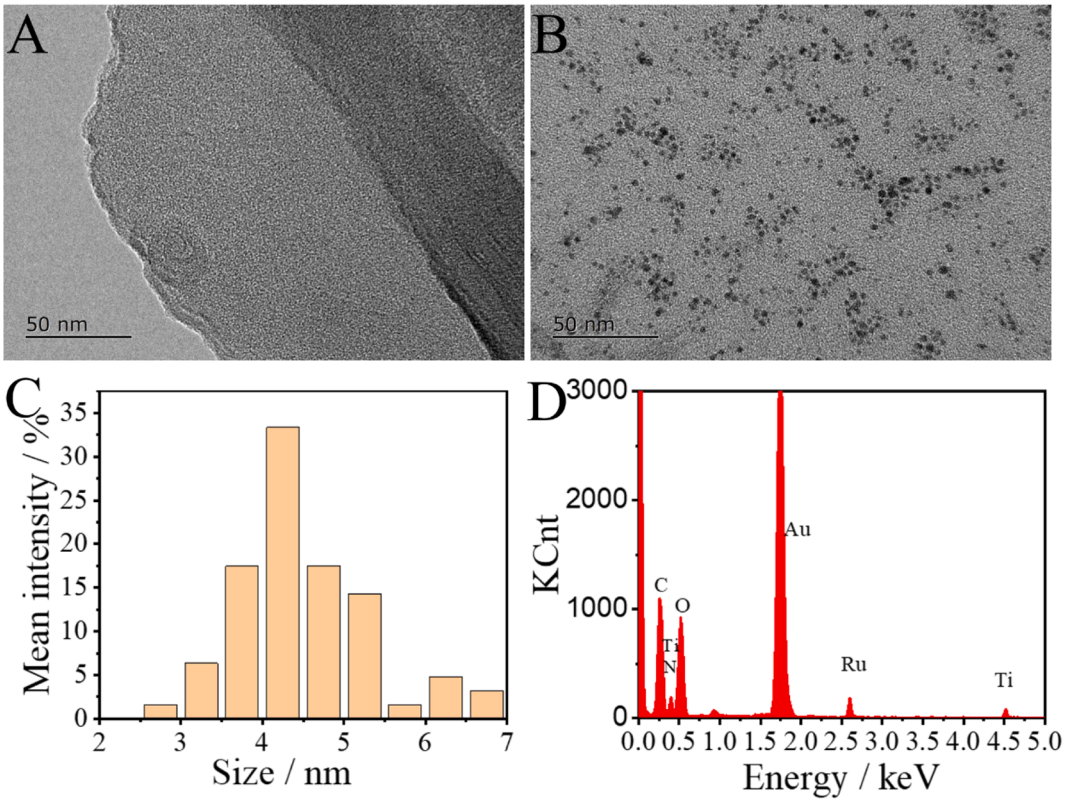

Fig. 3. (A) TEM characterization of Ti_3C_2. (B) TEM characterization of PEI-Ru@Ti_3C_2@AuNPs. (C) The corresponding size distribution diagram of (B). (D) The EDX spectrum of PEI-Ru@Ti_3C_2@AuNPs.

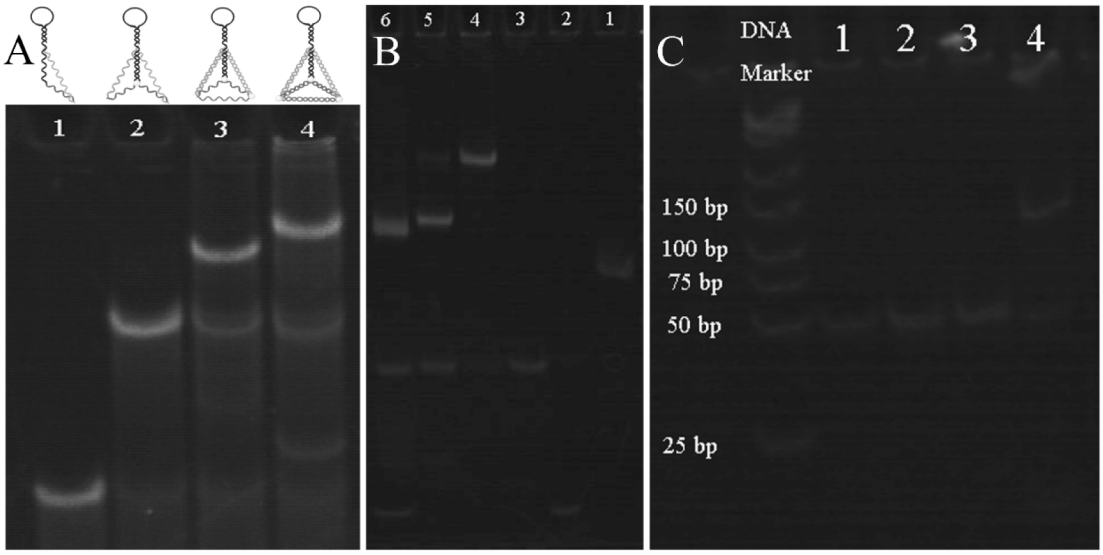

Fig. 4. Polyacrylamide gel electrophoresis analysis of (A) TDNAs construction process. Lane 1: S3, Lane 2: S3-S4, Lane 3: S3-S4-S5, Lane 4: S3-S4-S5-S6. (B) Entropy-driven cyclic amplification reaction, Lane 1: Scaffold, Lane 2: Blocker, Lane 3: Bandage, Lane 4: Substrate: Scaffold + Blocker + Bandage, Lane 5: Substrate + SARS-CoV-2 RdRp, Lane 6: Substrate + SARS-CoV-2 RdRp + Fuel. (C) Bipedal DNA walker, Lane 1: S1 probe, Lane 2: S2 probe, Lane 3: S1 + S2, Lane 4: S1 + S2 + Bandage.

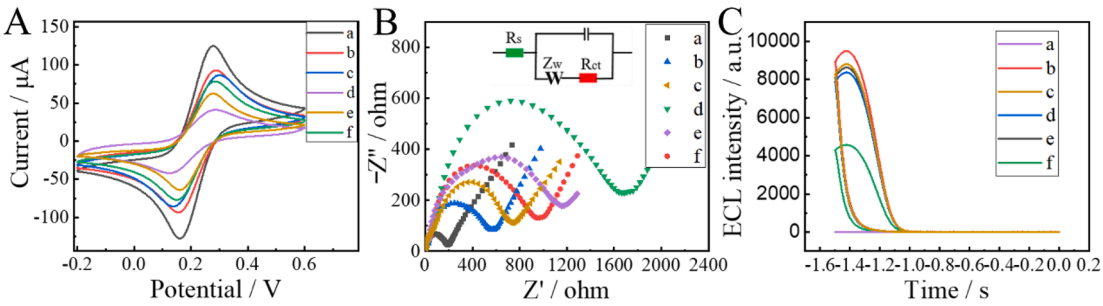

Fig. 5. Characterization of the stepwise construction process of the biosensor with CV (A), EIS (B) and ECL (C). (a) bare GCE, (b) GCE/Au-g-C_3N_4, (c) GCE/Au-g-C_3N_4/TDNAs, (d) GCE/Au-g-C_3N_4/TDNAs/MCH, (e) GCE/Au-g-C_3N_4/TDNAs/MCH treated with SARS CoV-2 RdRp and Nb.BbvCI, (f) Futher incubation with PEI-Ru@Ti_3C_2@AuNPs-S7. The inset in Fig. 5B was the modified Randles circuit to simulate the electrochemical process during electrode modification.

the PEI-Ru@Ti_3C_2@AuNPs-S7 probe (curve f) was modified to the modified electrode caused the peak current to be increased. Meanwhile, the effect of material modifications on the CV characteristics of the electrode was also explored, as shown in Fig. S3. In the absence of the co-reactant $S_2O_8^{2-}$ (curve a), the redox peak of the CV characteristic curve is very weak. However, when the co-reactant $S_2O_8^{2-}$ is present (curve b), the curve shows a strong redox peak at −1.1 V, which indicates that $S_2O_8^{2-}$ plays a significant role in the luminescence of C_3N_4. With the modification of TDNs (curve c) and MCH (curve d), the redox current gradually decrease. However, the peak of the electrode starts to increase when SARS CoV-2 RdRp and Nb.BbvCI (curve e) are involved in the reaction. In particular, the redox current further increases when PEI-Ru@Ti_3C_2@AuNPs (curve f) with excellent conductivity is modified to the electrode. The effect of material and DNA probe on the CV characteristics of the electrode is essentially the same as in the presence of 5 mM $[Fe(CN)_6]^{3-/4-}$, which mainly affects the electrode performance by influencing the electron transfer ability.

The construction process of the biosensor was characterized by EIS shown in Fig. 5B. The classically modified Randles circuit (inset in Fig. 5B) can simulate the electrochemical process of the modified electrode. The resistance of the electrode surface, the electron transfer and matter transfer during the redox process are mainly expressed through the resistance to charge transfer (Rct), which is precisely quantified especially through the Nyquist diagram's high-frequency semicircle [19]. The impedance value of the bare electrode (curve a) was the smallest. Continued to modify Au-g-C_3N_4 (curve b), TDNAs (curve c), MCH (curve d), and the impedance value gradually increased. When SARS-CoV-2 RdRp and Nb.BbvCI (curve e) presented, the TDNAs on the surface were clipped and the impedance value was slightly reduced. Finally, the suitable conductive PEI-Ru@Ti_3C_2@AuNPs-S7 probe (curve f) was modified on the electrode to obtain the impedance to be declined.

The ECL response to characterize the electrode modified with different substances was shown in Fig. 5C. The electrode was immersed in PBS solution containing 0.1 M $S_2O_8^{2-}$ for measuring. The bare electrode (curve a) had no ECL response. Spreading Au-g-C_3N_4 (curve b) with good luminescence performance on the surface of the electrode presented a higher ECL signal. When TDNAs (curve c) with poor conductivity and MCH (curve d) were modified on the electrode surface, the ECL signal gradually decreased. Subsequently, SARS-CoV-2 RdRp (curve e) was introduced and the ECL signal recovered slightly. Finally, the PEI-Ru@Ti_3C_2@AuNPs-S7 probe (curve f) was connected to TDNAs, and the ECL signal was reduced. Through these three methods, we could confirm that the biosensor was successfully constructed.

3.9. Optimization of analytical conditions

In order to obtain the optimal performance of the biosensor, some experimental parameters were optimized, including the concentration of S1 and S2 of the DNA walker, the dosage of Nb.BbvCI, the digestion time of Nb.BbvCI, and the incubation time of the entropy-driven

reaction. Fig. S4A depicted that as the concentrations of S1 and S2 increased, the ECL signal gradually decreased and tended to stabilize at 60 nM. Fig. S4B depicted that when the dosage of Nb.BbvCI reached 10 U, the ECL curve becomed stable. Fig. S4C showed that the optimal digestion time for Nb.BbvCI was 60 min. The optimal time for the entropy-driven reaction was 40 min as shown in Fig. S4D. Therefore, the concentration of S1 and S2 of DNA walker was selected to be 60 nM, 10 U and 60 min were used for the optimal dosage and optimal digestion time of Nb.BbvCI, and the optimal entropy-driven reaction time was 40 min.

3.10. Detection of SARS-CoV-2 RdRp with the ratiometric biosensor

Under the optimized conditions, the ratiometric ECL biosensor was used to detect SARS-CoV-2 RdRp gene. Fig. 6A depicted that the ECL signal intensity decreased at 460 nm and the ECL signal intensity increased at 620 nm as the concentrations of SARS-CoV-2 RdRp increased from 10 aM to 10 pM. Fig. 6A also described that the change of ECL signal intensity at 460 nm possessed an excellent linear relationship of $y = -502.82\ lgC_{(RdRp)} - 986.17$, $R^2 = 0.9944$. The change of ECL signal intensity at 620 nm also revealed an excellent linear relationship of $y = 805.79\ lgC_{(RdRp)} + 14704.28$, $R^2 = 0.9950$. Here y represents the ECL intensity at 460 nm or 620 nm and $lgC_{(RdRp)}$ represents the logarithmic value of RdRp concentration. In order to obtain higher reliability, we evaluated the logarithmic value of ECL (620 nm)/ECL (460 nm) as the concentration of SARS-CoV-2 RdRp increased, as shown in Fig. 6B. According to the limit of detection (LOD) = 3σ/k, the LOD was calculated as 7.8 aM. Compared with other methods in detecting DNA, our method possessed a lower detection limit, as shown in Table S2. Moreover, our method has a significant advantage in LOD, compared to other methods for SARS-CoV-2 detection (as shown in Table S3). The lower detection limits obtained result from our ratiometric ECL biosensing platform constructed on DNA tetrahedra, which combines the significant advantages of entropy-driven reactions and DNA walker cycling as signal amplification techniques. The conventional assays using molecular beacons (MBs) probes are shown schematically in Fig. S5. In the absence of target DNA, MBs exhibit a stem-loop structure that brings the attached fluorophore (Cy3) and quencher (BHQ-2) in close proximity, reducing the fluorescence emission. However, in the presence of target DNA, target DNA binds to MBs to form a hybrid complex, disrupting the stem-loop structure, which leads to the separation of Cy3 from BHQ-2, producing a large increase in fluorescence. By using the method with MBs, we obtained a LOD of 9.8 nM (see Fig. S6), which was much less sensitive than our method.

3.11. Stability and selectivity of the ratiometric biosensor

In order to evaluate the stability of the biosensor, the modified electrode was immersed in PBS containing 10 pM SARS-CoV-2 RdRp and scanned continuously for 16 cycles. It can see from Fig. 6C that the ECL signals remain stable at 460 nm with a relative standard deviation (RSD) of 2.34%, and at 620 nm with an RSD of 3.61%. In order to evaluate the selectivity of the ratiometric biosensor, some interferences were introduced. When the biosensor was immersed in 1 pM of SARS-CoV-2 RdRp, 100 pM of SARS-CoV RdRp, 100 pM of random DNA and blank. As shown in Fig. 6D, the biosensor processed by SARS-CoV-2 RdRp exhibited a significant distinction compared with the biosensor processed by other interferences. Therefore, the constructed biosensor possessed splendid selectivity.

3.12. Applicability of the biosensor in real sample analysis

It is necessary for the ratiometric biosensor to be used for early clinical detection. The recovery experiment was performed in 50-fold diluted human serum, shown in Table 1. The biosensor was carried out in different concentrations of SARS-CoV-2 RdRp serum, and it was

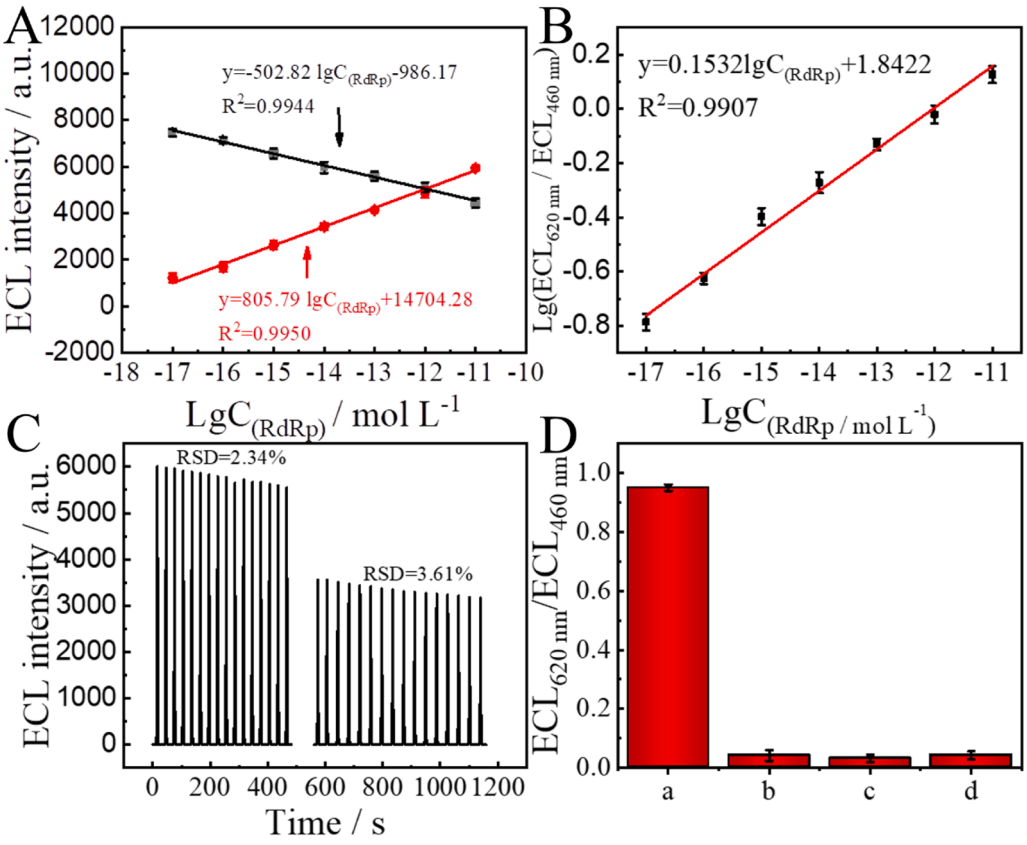

Fig. 6. (A) Relationship between the ECL intensity of (a) Au-g-C_3N_4 at 460 nm and (b) PEI-Ru@Ti_3C_2@AuNPs at 620 nm and the logarithmic value of SARS-CoV-2 RdRp concentrations (10 aM, 100 aM, 1 fM, 10 fM, 100 fM, 1 pM, 10 pM). (B) The calibration curve for SARS-CoV-2 RdRp. (C) Stability of the ECL biosensor with 16 continuous measurements at 460 nm (left) and 620 nm (right), respectively, with a SARS-COV-2 RdRp concentration of 10 pM. (D) Selectivity of ratiometric ECL biosensor at (a) 1 pM for SARS-CoV-2 RdRp, (b) 100 pM for SARS-CoV RdRp, (c) 100 pM for random DNA, (d) blank solution. The ECL measurement used a series of filters spaced 20 nm apart, measured in 0.1 M PBS (pH = 7.4) containing 0.1 M $S_2O_8^{2-}$.

Table 1
Recovery results for the assay of SARS-CoV-2 RdRp in 50-fold dilution of human serum.

Sample number	Added	Found	Recovery (%)	RSD (%, n = 3)
1	10 aM	9.45 aM	94.50	1.51
2	100 aM	101.35 aM	101.35	3.63
3	1 fM	0.97 fM	97.00	2.24
4	10 fM	10.25 fM	102.50	1.92
5	100 fM	103.56 fM	103.56	4.30
6	1 pM	0.92 pM	92.00	4.11
7	10 pM	9.79 pM	97.90	2.98

found that the recovery value was from 92.00% to 103.56%, and the RSD was from 1.51% to 4.30%. It exhibited that this biosensor could be applied to the detection of actual samples.

4. Conclusions

In summary, we reasonably designed a dual-wavelength ratiometer TDNAs ECL biosensor to detect SARS-CoV-2 RdRp gene combined with entropy-driven and bipedal DNA walker cycle amplification strategies. This ECL biosensor has the following advantages. First, in this ratiometric ECL biosensor, Au-g-C_3N_4 as an excellent donor and PEI-Ru@Ti_3C_2@AuNPs as an excellent acceptor were designed to achieve ECL-RET. Second, unlike the traditional DNA walker, the bipedal DNA walker walks on a walking track by bandage DNA combining two adjacent feet. However, two feet without the participation of bandage DNA cannot walk on the track because they are farther apart. Besides, TDNAs modified by hairpin structures act on the electrode surface as walking tracks for the bipedal DNA walker. Third, Ultra-sensitive detection was achieved by combining two amplification strategies, entropy-driven and bipedal DNA walker. The detection range of the biosensor can be from 10 aM to 10 pM, and the detection limit was as low as 7.8 aM. The dual-wavelength ratiometric ECL biosensor was used in human serum to exhibit an excellent recovery rate and could be used in early clinical diagnosis.

Declaration of Competing Interest

The authors declare that they have no known competing financial interests or personal relationships that could have appeared to influence the work reported in this paper.

Acknowledgment

This work was supported by the National Natural Science Foundation of China (21705061), the Jiangsu Provincial Key Medical Discipline (Laboratory) (ZDXKA2016017) and the Innovation Capacity Development Plan of Jiangsu Province (BM2018023).

Appendix A. Supplementary data

Supplementary data to this article can be found online at https://doi.org/10.1016/j.cej.2021.131686.

References

[1] L.J. Carter, L.V. Garner, J.W. Smoot, Y. Li, Q. Zhou, C.J. Saveson, J.M. Sasso, A. C. Gregg, D.J. Soares, T.R. Beskid, S.R. Jervey, C. Liu, Assay techniques and test development for COVID-19 diagnosis, ACS Central Sci. 6 (5) (2020) 591–605.
[2] T. Ji, Z. Liu, G. Wang, X. Guo, S. Akbar khan, C. Lai, H. Chen, S. Huang, S. Xia, B. o. Chen, H. Jia, Y. Chen, Q. Zhou, Detection of COVID-19: A review of the current literature and future perspectives, Biosens. Bioelectron. 166 (2020) 112455, https://doi.org/10.1016/j.bios.2020.112455.
[3] P. Moitra, M. Alafeef, K. Dighe, M.B. Frieman, D. Pan, Selective naked-eye detection of SARS-CoV-2 mediated by n gene targeted antisense oligonucleotide capped plasmonic nanoparticles, ACS Nano 14 (6) (2020) 7617–7627.
[4] A. Demeke Teklemariam, M. Samaddar, M.G. Alharbi, R.R. Al-Hindi, A.K. Bhunia, Biosensor and molecular-based methods for the detection of human coronaviruses: A review, Mol. Cell. Probe. 54 (2020) 101662, https://doi.org/10.1016/j.mcp.2020.101662.
[5] V.M. Corman, O. Landt, M. Kaiser, R. Molenkamp, A. Meijer, D.K. Chu, et al., Detection of 2019 novel coronavirus (2019-nCoV) by real-time RT-PCR, Eurosurveillance 25 (2020) 23.
[6] T. Wu, Y. Ge, K. Zhao, X. Zhu, Y. Chen, B. Wu, F. Zhu, B. Zhu, L. Cui, A reverse-transcription recombinase-aided amplification assay for the rapid detection of N gene of severe acute respiratory syndrome coronavirus 2(SARS-CoV-2), Virology 549 (2020) 1–4.
[7] S. Han, O. Ko, G. Lee, S.-W. Jeong, Y.J. Choi, J.B. Lee, Rapid diagnosis of coronavirus by RNA-directed RNA transcription using an engineered RNA-based platform, Nano Lett. 21 (1) (2021) 462–468.
[8] Z. Fan, B. Yao, Y. Ding, J. Zhao, M. Xie, K. Zhang, Entropy-driven amplified electrochemiluminescence biosensor for RdRp gene of SARS-CoV-2 detection with self-assembled DNA tetrahedron scaffolds, Biosens. Bioelectron. 178 (2021), 113015.
[9] L. Li, Y. Chen, J.-J. Zhu, Recent advances in electrochemiluminescence analysis, Anal. Chem. 89 (1) (2017) 358–371.
[10] C. Ma, Y. Cao, X. Gou, J.-J. Zhu, Recent progress in electrochemiluminescence sensing and imaging, Anal. Chem. 92 (1) (2020) 431–454.
[11] K. Zhang, Z. Fan, B. Yao, T. Zhang, Y. Ding, S. Zhu, et al., Entropy-driven electrochemiluminescence ultra-sensitive detection strategy of NF-κB p50 as the regulator of cytokine storm, Biosens. Bioelectron. 176 (2021), 112942.
[12] L. Zhang, C. Xiong, H. Wang, R. Yuan, Y. Chai, A sensitive electrochemiluminescence immunosensor for cardiac Troponin I detection based on dual quenching of the self-enhanced Ru(II) complex by folic acid and in situ generated oxygen, Sensor. Actuat. B-Chem. 241 (2017) 765–772.
[13] H. Jin, R. Gui, J. Yu, W. Lv, Z. Wang, Fabrication strategies, sensing modes and analytical applications of ratiometric electrochemical biosensors, Biosens. Bioelectron. 91 (2017) 523–537.
[14] L. Zhu, M. Zhang, J. Ye, M. Yan, Q. Zhu, J. Huang, X. Yang, Ratiometric electrochemiluminescent/electrochemical strategy for sensitive detection of microrna based on duplex-specific nuclease and multilayer circuit of catalytic hairpin assembly, Anal. Chem. 92 (12) (2020) 8614–8622.
[15] J. Ye, L. Zhu, M. Yan, Q. Zhu, Q. Lu, J. Huang, H. Cui, X. Yang, Dual-wavelength ratiometric electrochemiluminescence immunosensor for cardiac Troponin I detection, Anal. Chem. 91 (2) (2019) 1524–1531.
[16] Q.-M. Feng, Y.-Z. Shen, M.-X. Li, Z.-L. Zhang, W. Zhao, J.-J. Xu, H.-Y. Chen, Dual-wavelength electrochemiluminescence ratiometry based on resonance energy transfer between Au nanoparticles functionalized g-C_3N_4 nanosheet and $Ru(bpy)_3^{2+}$ for microRNA detection, Anal. Chem. 88 (1) (2016) 937–944.
[17] X.-L. Huo, N. Zhang, H. Yang, J.-J. Xu, H.-Y. Chen, Electrochemiluminescence resonance energy transfer system for dual-wavelength ratiometric miRNA detection, Anal. Chem. 90 (22) (2018) 13723–13728.
[18] J. Xu, Y.-H. Wang, Z. Wei, F.-T. Wang, K.-J. Huang, Significantly improving the performance of self-powered biosensor by effectively combining with high-energy enzyme biofuel cells, N-doped graphene, and ultrathin hollow carbon shell, Sensor. Actuat. B-Chem. 327 (2021), 128933.
[19] Z. Fan, Z. Lin, Z. Wang, J. Wang, M. Xie, J. Zhao, K. Zhang, W. Huang, Dual-wavelength electrochemiluminescence ratiometric biosensor for NF-κB p50 detection with dimethylthiodiaminoterephthalate fluorophore and self-assembled DNA tetrahedron nanostructures probe, ACS Appl. Mater. Interfaces 12 (10) (2020) 11409–11418.
[20] Q. Feng, M. Wang, X. Han, Q. Chen, B. Dou, P.o. Wang, Construction of an electrochemical biosensing platform based on hierarchical mesoporous NiO@N-Doped C microspheres coupled with catalytic hairpin assembly, ACS Appl. Bio Mater. 3 (2) (2020) 1276–1282.
[21] Y. Li, C.Z. Huang, Y.F. Li, Ultrasensitive electrochemiluminescence detection of microrna via one-step introduction of a target-triggered branched hybridization chain reaction circuit, Anal. Chem. 91 (14) (2019) 9308–9314.
[22] S. Lu, T. Hu, S. Wang, J. Sun, X. Yang, Ultra-sensitive colorimetric assay system based on the hybridization chain reaction-triggered enzyme cascade amplification, ACS Appl. Mater. Interfaces 9 (1) (2017) 167–175.
[23] C. Zhang, J. Chen, R. Sun, Z. Huang, Z. Luo, C. Zhou, M. Wu, Y. Duan, Y. Li, The recent development of hybridization chain reaction strategies in biosensors, ACS Sens. 5 (10) (2020) 2977–3000.
[24] Z. Zhang, S. Wang, J. Ma, T. Zhou, F. Wang, X. Wang, G. Zhang, Rolling circle amplification-based polyvalent molecular beacon probe-assisted signal amplification strategies for sensitive detection of B16 cells, ACS Biomater. Sci. Eng. 6 (5) (2020) 3114–3121.
[25] A. Abi, M. Lin, H. Pei, C. Fan, E.E. Ferapontova, X. Zuo, Electrochemical switching with 3D DNA tetrahedral nanostructures self-assembled at gold electrodes, ACS Appl. Mater. Interfaces 6 (11) (2014) 8928–8931.
[26] X. Yin, T. Hou, B. Huang, L. Yang, F. Li, Aptamer recognition-trigged label-free homogeneous electrochemical strategy for an ultrasensitive cancer-derived exosome assay, Chem. Commun. 55 (91) (2019) 13705–13708.
[27] L. Ge, W. Wang, F. Li, Electro-grafted electrode with graphene-oxide-like DNA affinity for ratiometric homogeneous electrochemical biosensing of microRNA, Anal. Chem. 89 (21) (2017) 11560–11567.
[28] X. Liu, M. Song, T. Hou, F. Li, Label-free homogeneous electroanalytical platform for pesticide detection based on acetylcholinesterase-mediated DNA conformational switch integrated with rolling circle amplification, ACS Sens. 2 (4) (2017) 562–568.
[29] F.-T. Wang, Y.-H. Wang, J. Xu, K.-J. Huang, Z.-H. Liu, Y.-F. Lu, et al., Boosting performance of self-powered biosensing device with high-energy enzyme biofuel cells and cruciform DNA, Nano Energy 68 (2020), 104310.

[30] J.L. Zhang, Y.H. Wang, K. Huang, K.J. Huang, H. Jiang, X.M. Wang, Enzyme-based biofuel cells for biosensors and in vivo power supply, Nano Energy 84 (2021), 105853.
[31] Y. He, L. Cheng, Y. Yang, P. Chen, B. Qiu, L. Guo, et al., Label-free homogeneous electrochemical biosensor for HPV DNA based on entropy-driven target recycling and hyperbranched rolling circle amplification, Sensor. Actuat. B-Chem. 320 (2020), 128407.
[32] F. Li, G. Li, S. Cao, B. Liu, X. Ren, N. Kang, et al., Target-triggered entropy-driven amplification system-templated silver nanoclusters for multiplexed microRNA analysis, Biosens. Bioelectron. 172 (2021), 112757.
[33] Y. Li, Y. Chu, Y. Li, C. Ma, L. Li, A novel electrochemiluminescence biosensor: Inorganic-organic nanocomposite and $ZnCo_2O_4$ as the efficient emitter and accelerator, Sensor. Actuat. B-Chem. 303 (2020), 127222.
[34] W. Yun, Y. Hu, Q. Liu, Y. Li, X. Wang, Y. Tang, et al., Thymine-Hg^{2+}-thymine coordination chemistry induced entropy driven catalytic reaction to form Hemin/G-quadruplex-HRP-mimicking DNAzyme for colorimetric and visual determination of Hg^{2+}, Spectrochim. Acta A 222 (2019), 117228.
[35] W. Yun, N. Li, R. Wang, L. Yang, L. Chen, Y. Tang, Proximity ligation assay induced hairpin to DNAzyme structure switching for entropy-driven amplified detection of thrombin, Anal. Chim. Acta 1064 (2019) 104–111.
[36] J. Chen, Z. Luo, C. Sun, Z. Huang, C. Zhou, S. Yin, et al., Research progress of DNA walker and its recent applications in biosensor, TrAC-Trend. Anal. Chem. 120 (2019), 115626.
[37] J.-L. Liu, Z.-L. Tang, J.-Q. Zhang, Y.-Q. Chai, Y. Zhuo, R. Yuan, Morphology-controlled 9,10-diphenylanthracene nanoblocks as electrochemiluminescence emitters for microrna detection with one-step DNA walker amplification, Anal. Chem. 90 (8) (2018) 5298–5305.
[38] S. Wang, Y. Ji, H. Fu, H. Ju, J. Lei, A rolling circle amplification-assisted DNA walker triggered by multiple DNAzyme cores for highly sensitive electrochemical biosensing, Analyst 144 (2) (2019) 691–697.
[39] Y. Huang, X. Zhu, C. Jin, W. Li, Y. Zhou, R. Yuan, Double-site DNA walker based ternary electrochemiluminescent biosensor, Talanta 219 (2020), 121274.
[40] Z. Liu, S. Lei, L. Zou, G. Li, L. Xu, B. Ye, Highly ordered 3D electrochemical DNA biosensor based on dual orientation controlled rolling motor and graftable tetrahedron DNA, Biosens. Bioelectron. 147 (2020), 111759.
[41] Z. Li, B. Zhao, D. Wang, Y. Wen, G. Liu, H. Dong, S. Song, C. Fan, DNA nanostructure-based universal microarray platform for high-efficiency multiplex bioanalysis in biofluids, ACS Appl. Mater. Interfaces 6 (20) (2014) 17944–17953.
[42] Y. Lin, J. Jia, R. Yang, D. Chen, J. Wang, F. Luo, L. Guo, B. Qiu, Z. Lin, Ratiometric immunosensor for GP73 detection based on the ratios of electrochemiluminescence and electrochemical signal using DNA tetrahedral nanostructure as the carrier of stable reference signal, Anal. Chem. 91 (5) (2019) 3717–3724.
[43] H. Chai, P. Miao, Bipedal DNA walker based electrochemical genosensing strategy, Anal. Chem. 91 (8) (2019) 4953–4957.
[44] K. Zhang, Z. Fan, B.o. Yao, Y. Ding, J. Zhao, M. Xie, J. Pan, Exploring the trans-cleavage activity of CRISPR-Cas12a for the development of a Mxene based electrochemiluminescence biosensor for the detection of Siglec-5, Biosens. Bioelectron. 178 (2021) 113019, https://doi.org/10.1016/j.bios.2021.113019.
[45] Z. Liu, S. Lei, L. Zou, G. Li, B. Ye, Grafting homogenous electrochemical biosensing strategy based on reverse proximity ligation and Exo III assisted target circulation for multiplexed communicable disease DNA assay, Biosens. Bioelectron. 167 (2020), 112487.
[46] Y. Wu, X. Li, X. Tan, D. Feng, J. Yan, H. Zhang, X. Chen, Z. Huang, H. Han, A cyclic catalysis enhanced electrochemiluminescence aptasensor based 3D graphene/photocatalysts Cu_2O-MWCNTs, Electrochim. Acta 282 (2018) 672–679.